

Examination of linear radiation propagation with the method of Laguerre-Gauss function

A. DUBIK, J. OWSIK, A. SARZYŃSKI

Kaliski Institute of Plasma Physics and Laser Microfusion, P.O. Box 49, 00-908 Warszawa, Poland.

The way of solving a stationary and uniform parabolic equation (describing diffraction of radiation) which employs the eigenfunctions of this equation has been described. The cylindrical symmetry of the beam has been assumed. The effect of the number of the used eigenfunctions on the accuracy of the initial condition approximation has been examined. The comparisons of the results of the method presented with those obtained by using the difference method are given. The described method has been illustrated by two examples: modelling of the laser beam decoherencing and the spatial filtering.

1. Introduction

Laser systems used in the research carried out in such fields as thermonuclear synthesis, isotopes separation, X-ray lithography etc., should be of relatively high power and energy as well as of uniform distribution of the power density across the cross-section of the beam and of small phase deformation. The laser system should be marked by the high total efficiency, i.e., by the high possible ratio of the output radiation energy to the energy supplied from the network. Therefore, the contemporary laser systems comprise many elements such as soft diaphragms, retransmitters, spatial filters, Faraday isolators, all kinds of diaphragms, and so on, in order to improve the beam quality and to enhance the amplification effectiveness. This results in a significant complexity of the high power laser system design, the mathematical description of which may be carried out with the use of the numerical methods exclusively.

One of such methods applied to the description of the laser channel is the difference method. In accordance with the data reported in paper [1] this method is not very efficient due to low eigenfrequencies of the algorithm and long computing time. The calculations of radiation propagation through space filters is especially laborious. For example, the laser system containing 4 space filters and 8 amplifying rods requires the computing time of 12 hours (for MERA-400 or IBM PC/XT computers) while 80% of that time is needed just for calculation of the radiation propagation in spatial filters.

The fundamental reason for which the difference method is still used quite frequently is that it requires a relatively small operational computer memory on one hand, and that all the field transformations such as amplification, self-focusing or

diffraction on apertures may be easily performed with merely slight increase of the computing time, on the other hand. The time-consumptions of the method when calculating the filters and great errors of numerical nature, appearing due to their cumulation along the whole propagation trajectory of the beam encourage to look for other quicker and more accurate numerical methods. From the methods possible to apply, like: Hankel transform, fast Hankel transform [2], eigenfunction method [3], fast Fourier transform [4], the method of fast Hankel transform and the method of eigenfunctions require equally small operational computer memory as that of differences if restricted to the axial symmetric beams only. Therefore, if the available computers are of small operational memory the methods saving memory should be applied.

In the present paper, the method of eigenfunctions has been used for the case of axial-symmetric beams. In this case, the parabolic equation has the solution expressed in terms of a series of Laguerre–Gauss functions. The additional reason, speaking for the application of this method (in place of that of fast Hankel transform) is the fact that it may be easily generalized to the case of angularly nonuniform beams. In the present work we apply the algorithm of parabolic solution analogical to that described in paper [5]. The only difference consists in application of Laguerre–Gauss function in place of Hermite–Gauss functions. Therefore, we do not intend to describe the algorithm solution in detail. Our aim is rather to provide a general presentation of the method (Sect. 2). In Section 3 the results of approximation of the selected functions with the help of finite sum of Laguerre–Gauss functions are presented, while in Sect. 4 the examples of application of the described method are shown.

2. Mathematical fundamentals of the Laguerre–Gauss functions

The parabolic equation applied commonly to the analysis of radiation propagation in the laser systems has the forms:

$$2ik \frac{\partial E}{\partial z} + \frac{1}{r} \frac{\partial}{\partial r} \left(r \frac{\partial E}{\partial r} \right) = 0, \quad (1)$$

$$\lim_{r \rightarrow 0} \frac{\partial E}{\partial r} = 0, \quad \lim_{r \rightarrow \infty} E(r) = 0 \quad (2)$$

where: $k = 2\pi/\lambda$ – wavenumber,

E – complex amplitude of the electric field, strength of the wave,

z – coordinate along the beam axis describing the direction of the radiation propagation,

r – current radius in the beam cross-section.

Both the stationary approximation and axial symmetry of the beam have been assumed. Equation (1) with conditions (2) has the eigenfunction of the form (the so-called

Laguerre–Gauss function)

$$f_n(r, z) = \frac{w_0}{w} L_n\left(2\frac{r^2}{w^2}\right) \exp\left\{-\left(\frac{r}{w}\right)^2 - i\frac{kr^2}{2R} - i(2n+1)\Phi\right\} \quad (3)$$

where: $L_n(x)$ – Laguerre polynomial of n -th order,

$$w^2 = w_0^2 \left[1 + \left(\frac{2z}{D}\right)^2\right], \quad (4)$$

$$R = -z \left[1 + \left(\frac{D}{2z}\right)^2\right], \quad (5)$$

$$\Phi = \arctan\left(\frac{2z}{D}\right), \quad (6)$$

$$D = kw_0^2. \quad (7)$$

Equation (1) and the boundary conditions (2) impose no conditions on the parameter w_0 (the radius of the Gaussian beam waist), i.e., eigenfunction of the zeroth order. It may be selected arbitrarily, which makes it possible to increase the accuracy of the calculations (see Sect. 3).

Equation (1) with boundary condition (2) and the initial condition

$$E(r, z)|_{z=0} = E_0(r) \quad (8)$$

has the solutions:

$$E(r, z) = \sum_{n=0}^{\infty} C_n f_n(r, z), \quad (9)$$

$$C_n = \int_0^{\infty} E_0(r) f_n^*(r, 0) r dr \quad (10)$$

where: C_n – complex (in general) coefficients of the initial condition expansion (8) into a series of the eigenfunction,

* – means complex conjugate.

In practical realization the finite sum is used in place of the infinite one

$$E(r, z) \simeq \sum_{n=0}^N C_n f_n(r, z). \quad (11)$$

This approximate solution generalized with the help of Talanov transformation [5] into either the convergent beam (focused by the lens) or the divergent ones enables us to design an effective numerical method for modelling of the radiation propagation in the laser systems.

3. Approximation of the unity jump function and supergaussian function by means of the finite sum of the Laguerre-Gauss function. A comparison with the difference method

The replacement of the infinite sum (9) by the finite one (11) introduces an error of approximation depending on the number N of components and on the quantity

$$r_m = a/w_0, \quad (12)$$

i.e., the ratio of the beam radius a to the radius of the waist of the Gaussian beam w_0 . As it is well known from the theory of numerical methods, the slow-varying functions may be approximated with high accuracy by means of the finite sum (11). When the calculations concern the lasers an important role is played by the functions of unity-jump

$$E_0(r) = \begin{cases} 1, & r \leq a \\ 0, & r > a \end{cases} \quad (13)$$

describing the transmission of diaphragm and pinhole located in the laser system. For this function, the coefficient of the expansion (10) may be calculated from the following recurrence formulae:

$$C_0 = 2[1 - \exp(-x_m/2)], \quad (14)$$

$$C_1 = 2x_m \exp(-x_m/2) - C_0, \quad (15)$$

$$C_{n+1} = \frac{[-C_n + nC_{n-1} + 2x_m \exp(-x_m/2) L_n(x_m)]}{n+1} \quad (16)$$

for $n \geq 1$, where

$$x_m = 2r_m^2. \quad (17)$$

In Figure 1 some selected eigenfunctions (of order $n = 3$ and $n = 10$, respectively), have been plotted for the two values $r_m = 1$ and $r_m = 4$. It can be seen that the frequency of oscillation of eigenfunctions increases with the increase of r_m , and consequently the fast-varying functions may be approximated more accurately. In this figure, the broken line is used to plot the approximate unity-jump function. The beam radius has been assumed to be equal to unity.

In Figure 2 the result of function approximation (13) has been plotted with the help of finite sum (11) for $r_m = 1$, for 20 components being summed up (Fig. 2a) and 200 (Fig. 2b). We can see that the increase of the number of components improves significantly the quality of approximation. For $N = 20$, rms error of approximation amounts to about 5%, while for $N = 200$ it is reduced to 1.6%. Now, in Fig. 3 the same functions have been plotted for $r_m = 4$. The rms error for $r_m = 4$ and $N = 200$ amounts to 1.6%, while for $N = 200 - 0.4\%$. Hence, we conclude that the increase of both the number of components and the value of r_m results in an improvement of the approximation quality, i.e., significant diminishing of the rms error.

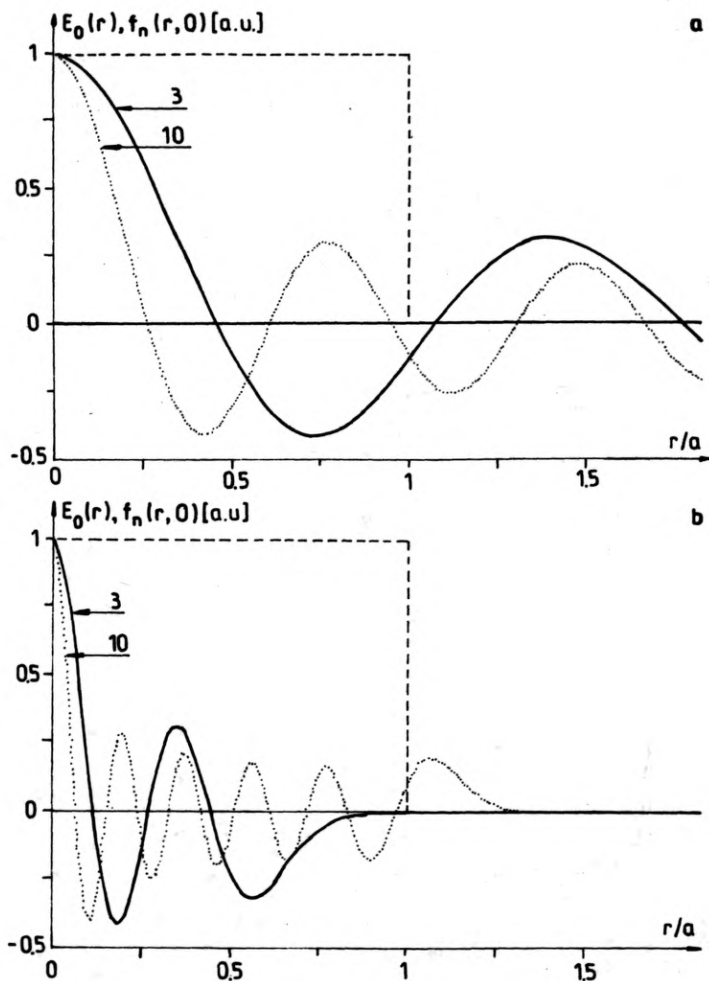


Fig. 1. Influence of r_m ratio of the beam a to the radius of the Gaussian beam w_0 on the oscillation speed of the selected eigenfunctions $n = 3$ and $n = 10$. The unity-jump function (Eq. (13)) has been plotted with a broken line for: **a** - $r_m = 1$, **b** - $r_m = 4$

In contrast to the rms error which diminishes while both the number of the components and r_m increase, the maximal error of approximation remains constant and amounts to about 10% (strictly speaking, oscillates within the range 8–12%). This error may be reduced in two ways. The first one employs the so-called Tichonov regularization, which practically consists in a change of the values of the expansion coefficients ((14)–(16)). Namely, in place of the coefficients (14)–(16) we apply those changed according to the formula

$$C'_n = C_n / (1 + \varepsilon n), \quad \varepsilon \ll 1 \quad (18)$$

where the value of ε should be chosen from the range of 10^{-4} – 10^{-2} .

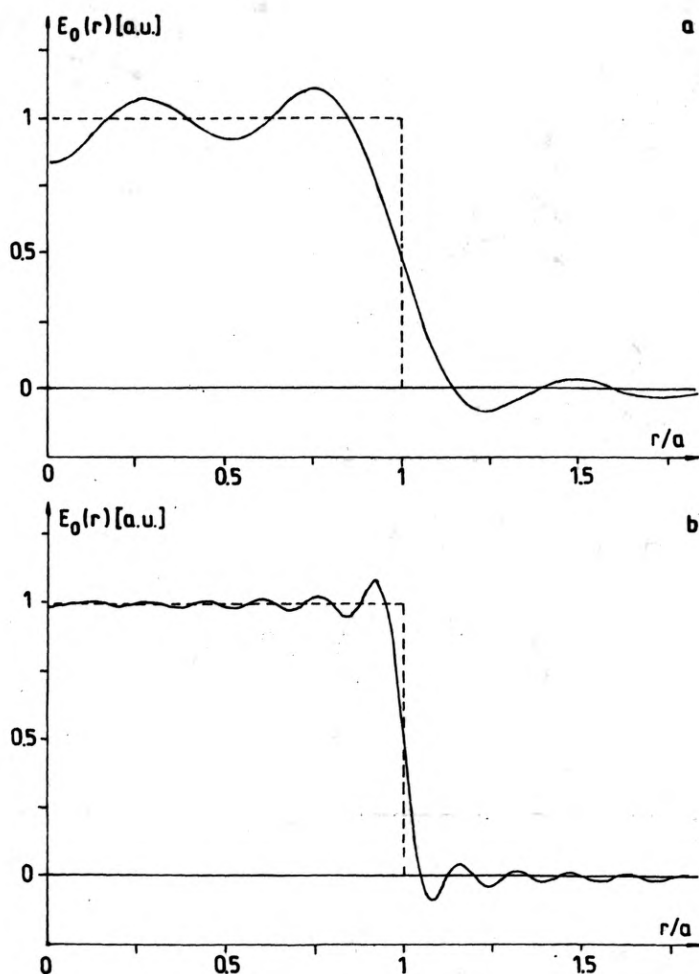


Fig. 2. Approximation of the unity-jump function with the help of the finite sum of eigenfunctions: a - $N = 20$, b - $N = 200$. $r_m = 1$ has been assumed. The broken line is used to plot the approximated function while the continuous line shows the result of approximation

The other way is to replace the real function by another one, for instance, the supergaussian function and expand the latter into series (Fig. 4). In Figure 4a the result of approximation has been plotted after application of the Tichonov regularization. The result of the approximation of the supergaussian function done with the aid of summing up of 100 eigenfunctions, is shown in Fig. 4b

$$E_0(r) = \exp[-3.455(r/a)^{100}]. \quad (19)$$

In this case, the coefficients of the expansion have been obtained by performing the numerical integration (10).

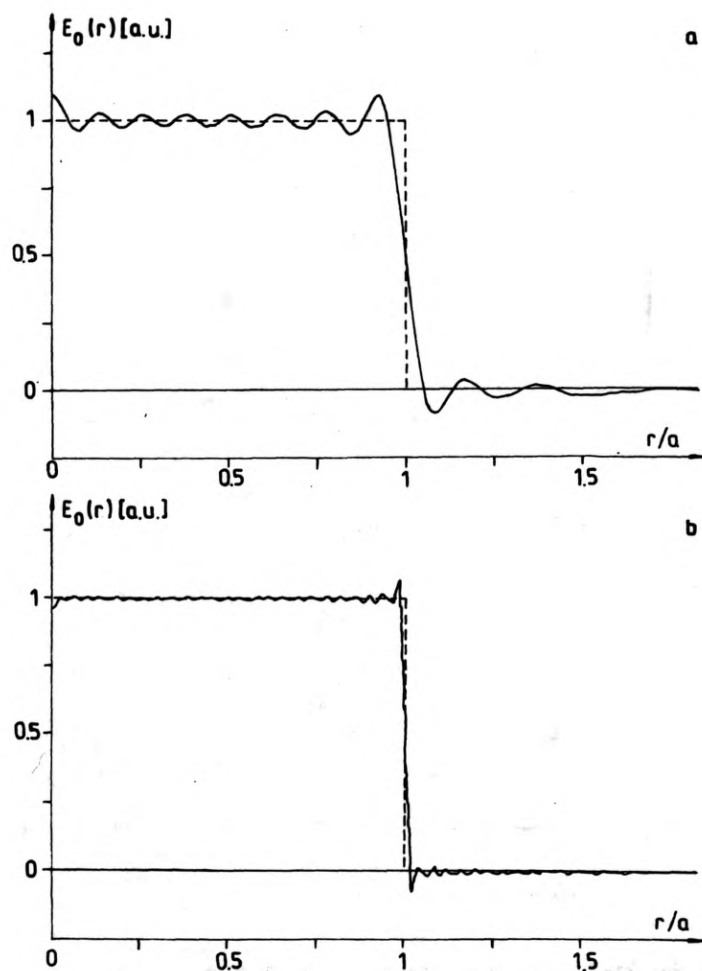


Fig. 3. Approximation of the unity-jump function with the help of finite sum of eigenfunctions: **a** — $N = 20$, **b** — $N = 200$. $r_m = 4$ has been assumed. The broken line is used to plot the approximated function while the continuous line shows the result of approximation

Of these two ways of removing oscillations from the approximating function connected with the Gibbs effect the one consisting in expansion of the supergaussian function (instead of unity-jump) into a series seems to be more safe.

The further calculations have been carried out without any regularization since it has been stated that in the planes $z > 0$ and for $N > 200$ the influence of the number of terms on the solution was small. For instance, the increase of the numbers of terms from $N = 200$ to $N = 400$ for $r_m = 10$ changed the solution by single percent corrections.

It should be emphasized that the oscillations of the approximating functions

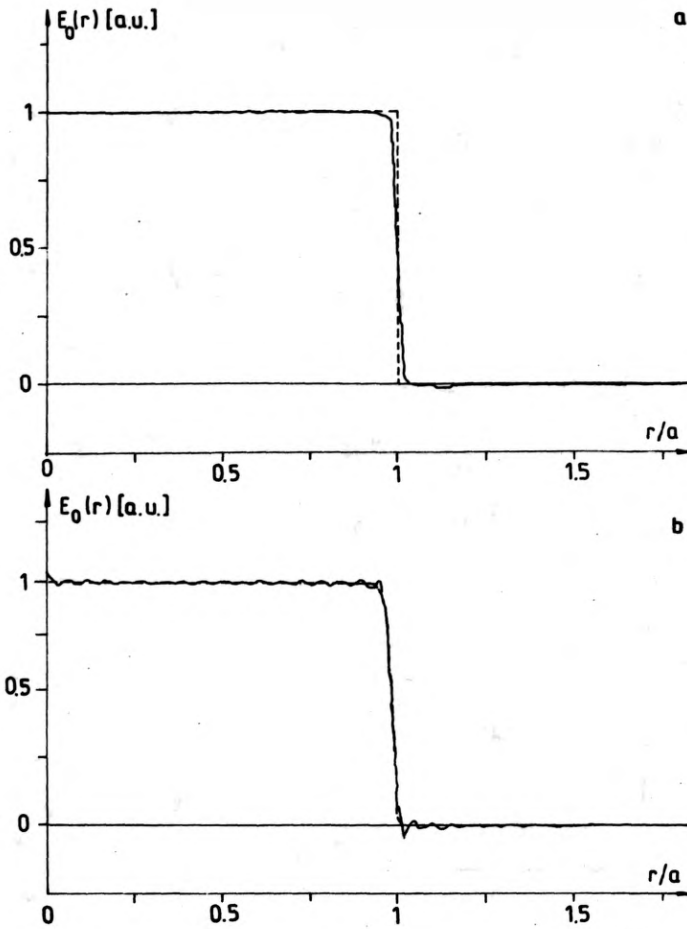


Fig. 4. Improvement in approximation of the unity-jump function with the help of finite sum of eigenfunctions. **a** – regularization due to Tichonov method (Eq. (18)), $N = 1000$, $r_m = 4$, $\varepsilon = 0.001$, **b** – approximation of the supergaussian function (Eq. (19)), $N = 100$, $r_m = 4$

around the approximated one (for the discussed eigenfunctions) are of much higher frequencies than those in the difference method [1]).

So far, the conditions of accurate approximation of the unity-jump function have been examined by using a finite sum of eigenfunctions. It is also interesting to compare the presented method with both the analytic solutions and those obtained with the help of difference method [1]. In order to compare the two methods, the calculations modulating the propagation of the axial-symmetric beam in the spatial filter have been carried out. A rectangular distribution of the power density in the beam at the object plane of the filter has been examined. The comparison has been made in three planes of filter:

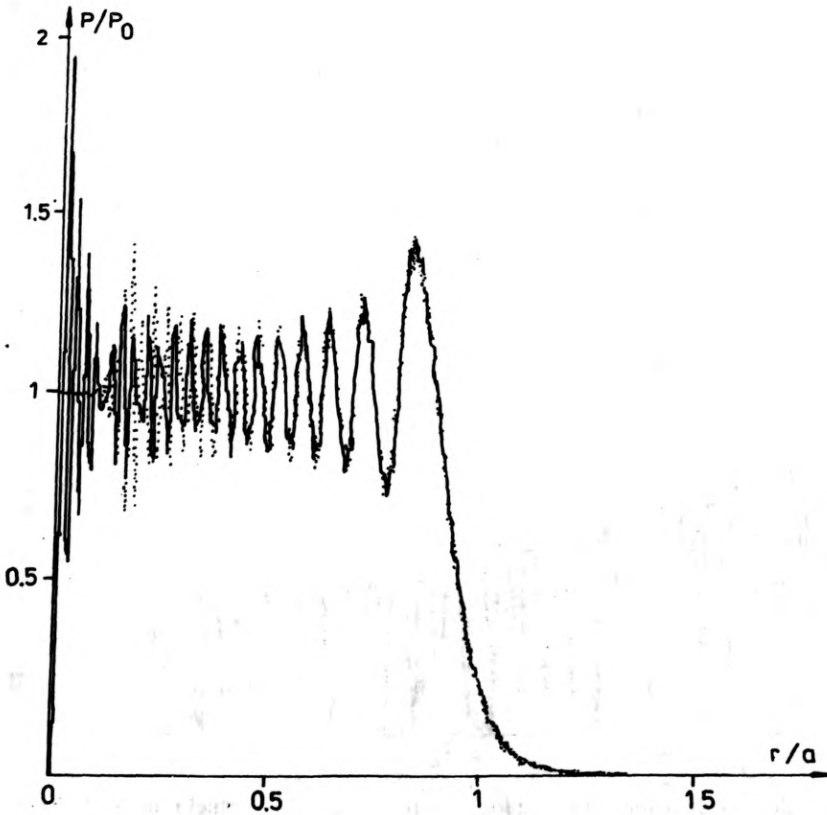


Fig. 5. Comparison of the diffraction distributions of the power density in the beam for the Fresnel number $S_f = 40$. Continuous curve – solution obtained by using the method of eigenfunctions, $N = 500$, $r_m = 10$; dotted curve – solution obtained by using the difference method

- in the near zone (Fresnel number $S_f = 40$, Fig. 5),
- in the far zone ($S_f = 0$, Fig. 6),
- in the image plane of filter ($S_f = \infty$, Fig. 7).

The solution obtained with the method of the eigenfunctions (ME) has been plotted with a continuous line while that obtained with the difference method (DM) – with a dotted line.

In the near zone ($S_f = 40$, Fig. 5) the solution ME takes the zero value (precisely $\approx 10^{-5}$) on the beam axis. The number of diffraction maxima along the beam radius amounts to 20. These facts are consistent with the diffraction theory. The application of the regularization of the coefficients of the series results in smoothing the solution, in increasing the value of the power density on the beam axis and even in diminishing the number of diffraction peaks if the value of ε is too high (18). For these reasons, we have resigned from the regularization of the coefficients of the series. The solution DM is consistent with that of ME only at the rim of the beam.

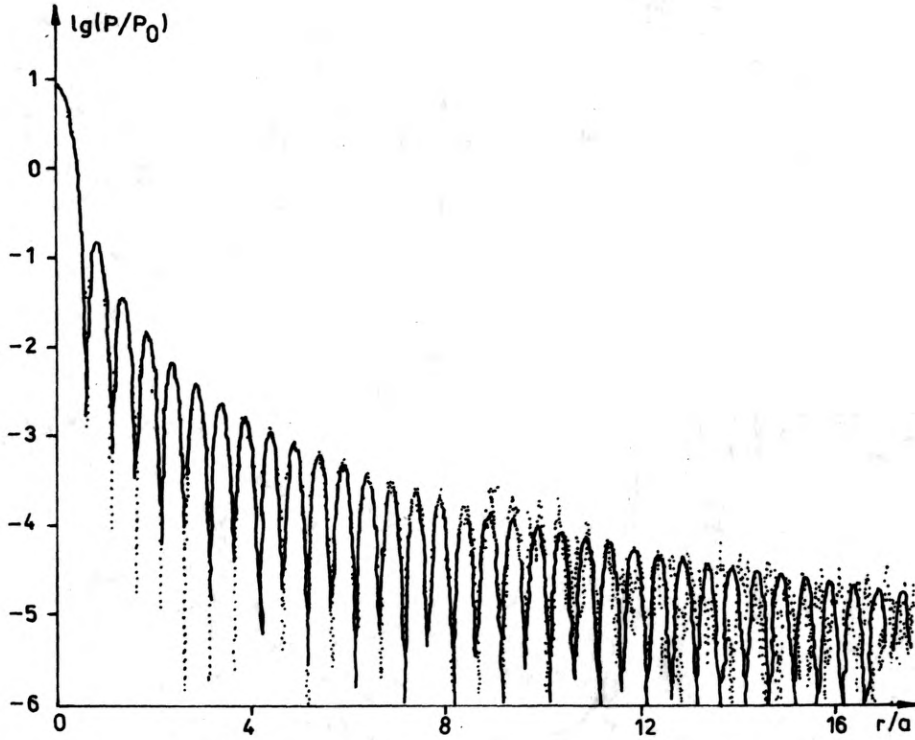


Fig. 6. Comparison of the power density distribution in the focal plane of the lens. Fresnel number $S_f = 0$. The others as in Fig. 5

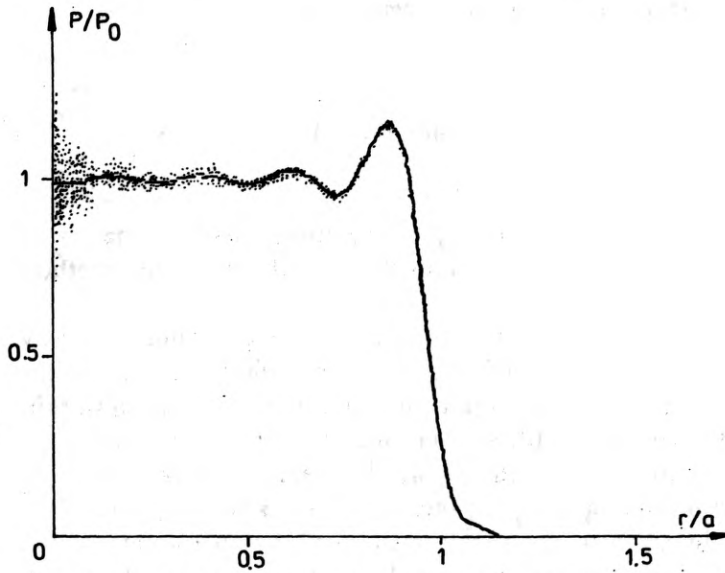


Fig. 7. Comparison of the power density distribution in the image plane of the filter $S_f = \infty$. The others as in Fig. 5

DE reproduces faithfully only 6–7 extreme diffraction maxima. The other peaks do not appear at all. From Fig. 5 it follows that in DM the central part of the beam remains unperturbed. When reducing the spatial step Δr in DM and increasing the number of network knots the range of consistency of both solutions may be broadened — this occurs, however, at the expense of significant elongation of the computing time (proportionally to Δr^{-3}). Both solutions presented have been obtained after about 40 min computing time on the IBM PC/XT microcomputer (20 min for each solution).

In the far zone (Fig. 6, Fresnel number $S_f = 0$, lens focus), the solution ME was consistent with the analytic solution with the accuracy up to first three significant digits within the whole range of arguments $r/a < 20$. The DM solution is consistent with the ME solution only in the central part (7–9 diffraction orders). In some points the amplitude of the solution DM is 3 times as great as the accurate value.

In the image plane of the filter (Fig. 7) the DM solution oscillates around the EM solution with the period equal to the step Δr of the network. Such small-scale parasitical perturbations of the DM solution are characteristic for this method.

The above considerations allow us to state that by using EM much more accurate solutions may be obtained than with the use of DM.

4. Examples of eigenfunction method application to determination of the laser beam distribution

We shall consider two examples of the application of the method to analysis of the laser beam propagation, i.e., decoherencing and filtration.

As the first one, the problem of decoherencing of the laser beam will be considered. The decoherencing is realized by locating the elements perturbing the phase distribution in the beam trajectory in such a way that the beam of radiation splits into many component beams incoherently interacting with each other. The decoherencing causes an improvement of illumination uniformity of microspheres in the experiments concerning the thermonuclear synthesis, a decrease of self-focusing, and increase of energy extraction from the laser amplifiers.

At the Institute of Physics of the Academy of Sciences, USSR, a number of experiments have been carried out, in which the decoherencing element was the Michelson pile composed of eighteen circular glass plates of 3 mm in thickness and different radii. The smaller had an 11 mm diameter while each subsequent plate was of diameter greater by 2 mm than the previous one [6].

Such a design of the pile assured the decoherency of the Delphin laser beam (corresponding to the spectrum width and the degree of time coherence). Due to technological reasons the transmission of this pile was the function of the type

$$T(r) = \left. \begin{array}{l} 1, \quad r \leq 5.35 \quad \text{or} \quad 5.5+i \leq r \leq 6.35+i \\ 0, \quad 5.35+i < r < 5.5+i \end{array} \right\}, \quad (20)$$

$i = 0, 1, 2, \dots$, and so on, r [mm] (the plates were provided with the so-called

technological phase of widths 0.15 mm which "threw away" a part of the radiation outside the beam). This pile causes the splitting of the incident beam into eighteen component beams (among those 17 being of ring form) interacting incoherently with each other.

The following manner of modelling of decoherencing influence of the pile on the laser beam has been assumed. The phase delay between the component beams has been neglected, the above presented method of eigenfunctions has been applied, the power density distributions of the radiation appearing as a result of the diffraction of eighteen mutually independent beams (including seventeen ring beams) have been calculated. Incoherent interaction of the beams was modelled through summing up the laser beam power densities of the component beams (instead of the complex amplitudes of the electric field strength of the wave) to obtain the power density of the total beam.

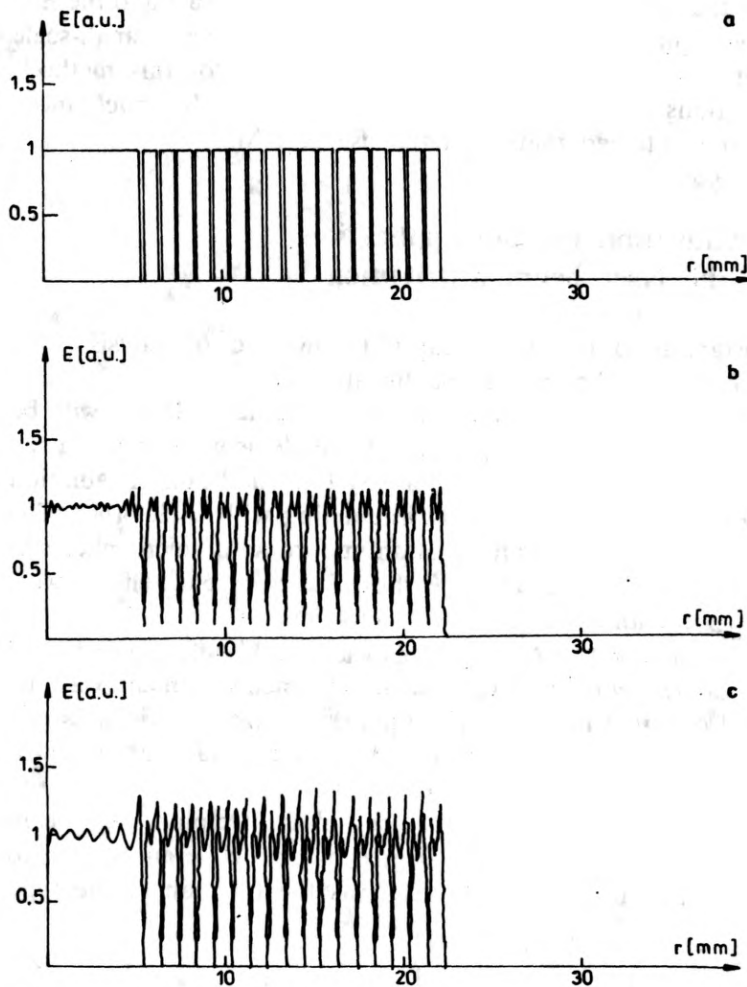


Fig. 8. Transmission of the Michelson pile applied to decoherencing the laser beams. **a** — assumed transmission of the pile, **b** — transmission obtained in calculations when summing up 200 terms in the series, **c** — transmission obtained in calculations when summing up 400 terms in the series

The results obtained are consistent with those achieved in experiments. The focusing influence of the pile on the beams was observed at the distance greater than 10 m from the pile. A satisfactory quantitative consistence of the used numerical model with experiment has been proved by comparing the numerical solution with the experimental results for the distance of 2 m from the pile. In the far zone (i.e., in the focus of the lens) such a good consistence has not been achieved, which may be explained by the fact that the beam incident on the pile was partially coherent, which has not been taken into account in our calculations.

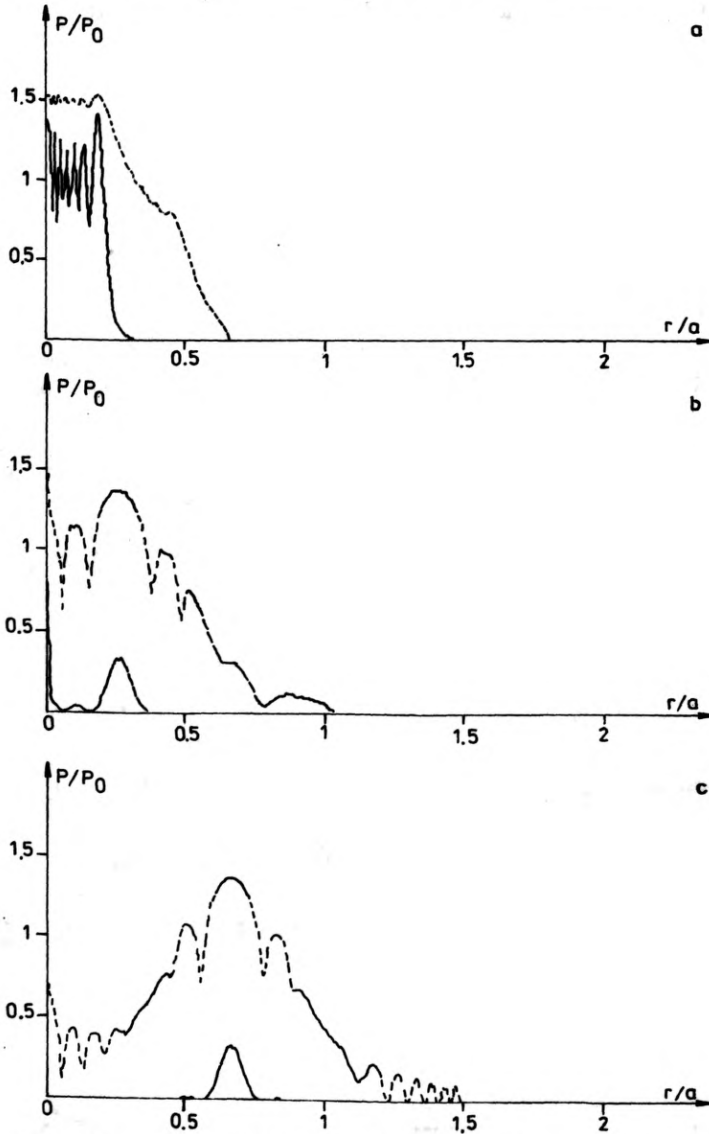


Fig. 9. Power density distribution of the radiation for chosen component beams at the distance of 2 m from the pile. a — central beam $r_{int} = 0$, $r_{ext} = 5.35$ mm, b — ring beam $r_{int} = 5.5$ mm, $r_{ext} = 6.35$ mm, c — ring beam $r_{int} = 15.5$ mm, $r_{ext} = 15.35$ mm. The lower curves — linear scale, the upper curves — logarithmic scale (a unity interval on the vertical scale corresponds to four orders of magnitude)

Below, the selected results of calculations will be discussed. In Figure 8 the amplitude transmission of the Michelson pile has been plotted. In Figure 8a the assumed transmission has been drawn while in Figs. 8b and 8c that obtained by numerical calculations is presented (b — for $N = 100$, c — for $N = 400$). A comparison of Figs. 8b and 8c leads to a surprising result that the doubling of the number of the terms worsened the quality of approximation. It should be remembered that the solutions from Figs. 8b and 8c have been obtained after summing up eighteen component beams. Unfortunately, this gives no explanation of the observed worsening of the approximation. In all the further graphs the lower

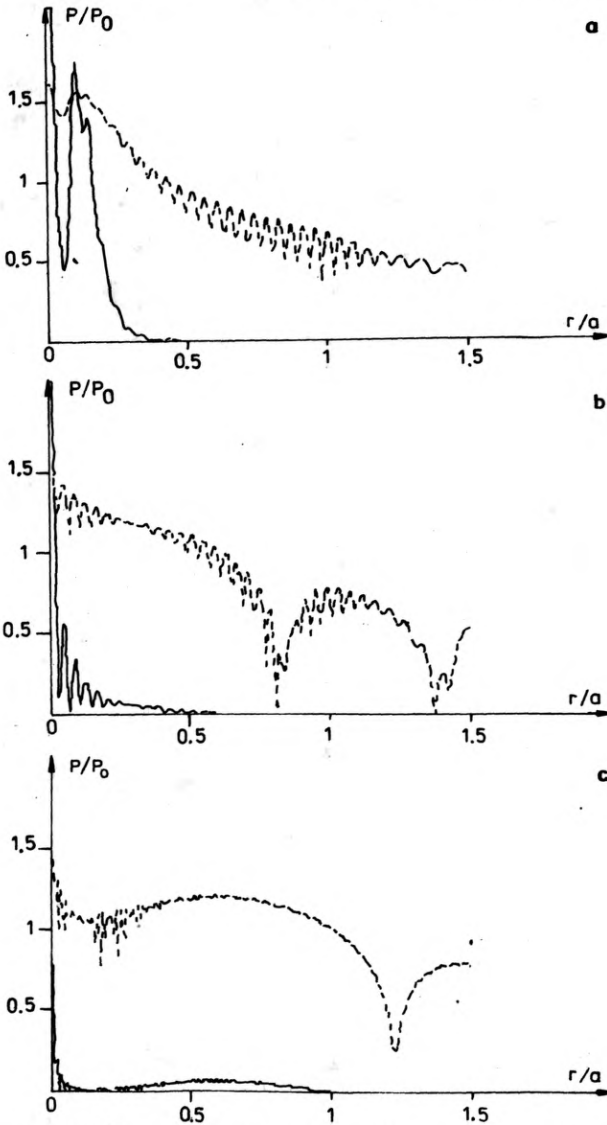


Fig. 10. Power density distribution of the radiation for chosen component beams at the distance of 10 m from the pile. The others as in Fig. 9

curves are drawn in the linear scale while the upper ones in the logarithmic scale (the vertical segment of unity length corresponds to four orders).

In Figure 9 the distributions of three chosen component beams at the distance of 2 m from the pile are plotted, while the same for the distance of 10 m is shown in Fig. 10. The small scale modulations of the radiation power density seen in Fig. 10 is worth noting. In the difference method a correct quantitative description is practically impossible.

In Figure 11 the power density distribution in the total beam has been plotted for the distance of 2 m from the pile: **a** – under the assumption of the coherence of the component beams, i.e., the complex amplitudes of the electric fields have been summed up; **b** – under assumption of lack of coherence, i.e., the intensities of the component beams have been summed up.

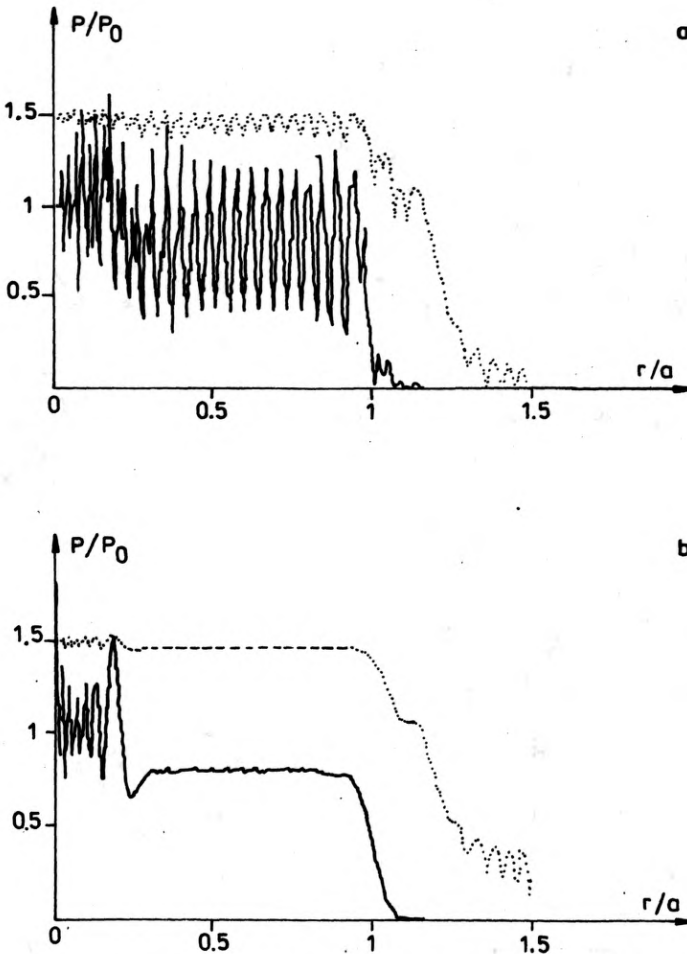


Fig. 11. Power density distributions in the total beam at the distance of 2 m from the pile. **a** – coherent adding, **b** – incoherent adding. The continuous curve – linear scale, dotted curve – logarithmic scale (a unity interval in the vertical scale corresponds to four orders of magnitude)

A quantitative change in the distributions in those two cases has been observed while the "incoherent" summing up results in much more uniform distributions. The distribution in the total beam at the distance of 10 m from the pile has been shown in Fig. 12. A concentration of energy at the beam axis (Fig. 12b) is visible. This effect is more distinct at greater distance from the pile.

As a subsequent example of application of our method we shall consider the filtration of radiation. The filter taken to the calculations was composed of two lenses of common focus and of focal length $f = 1000$ mm and the pinhole located near the beam focus. A circular source of the plane electromagnetic wave was positioned in front of the first lens of the filter at the distance of 1000 mm from the latter. The image of this source appears at the distance of 1000 mm behind the second lens of the filter.

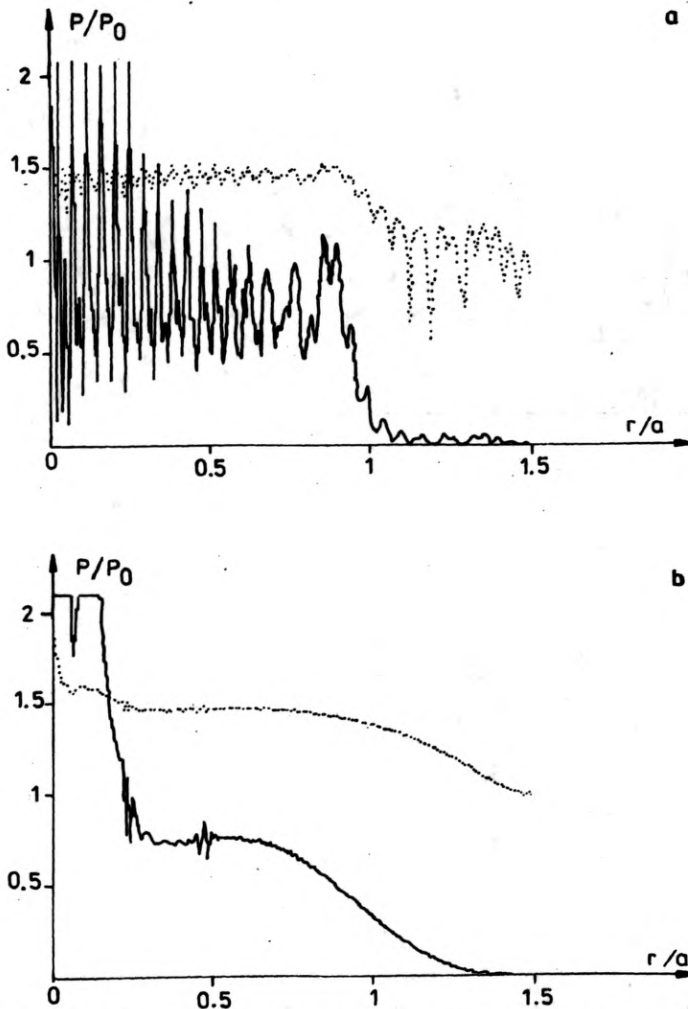


Fig. 12. Power density distribution in the total beam at the distance of 10 m from the pile. The others as in Fig. 11

In Figure 13a the result of approximation of the unity-jump function is shown, which was obtained by summing up 500 terms of the series of the Laguerre–Gauss functions. The lack of oscillations of approximating function follows from a small number of points for which the field was calculated (100 points on the fragment of 20 mm length). In Figure 13b the power density of the filter focus has been plotted. In Figure 14 the influence of the pinhole located at the filter focus on the radiation distribution in the image plane is demonstrated for several radii of the pinhole. The pinhole radii have been chosen in such a way that:

i) The pinhole stops the second and higher order fringes of the Airy's distribution at the focus $r_{\text{pinh}} = 0.12$ mm.

ii) The pinhole stops the third and higher order Airy fringes, $r_{\text{pinh}} = 0.17$ mm.

iii) The pinhole stops the fourth and higher order Airy fringes, $r_{\text{pinh}} = 0.22$ mm.

As the pinhole radius increases the distribution of radiation at the image plane approaches the initial distribution.

The fundamental results of this series of calculations may be summed up as follows. If an even number of side orders (Airy fringes) passes through the pinhole a maximum appears on the axis of the beam in the image plane, while for an odd number a minimum occurs. The amplitude of oscillations diminishes and their frequency increases for increasing radius of the pinhole. This results from cutting out the high frequency part of the beam spectrum by the pinhole — which is a well

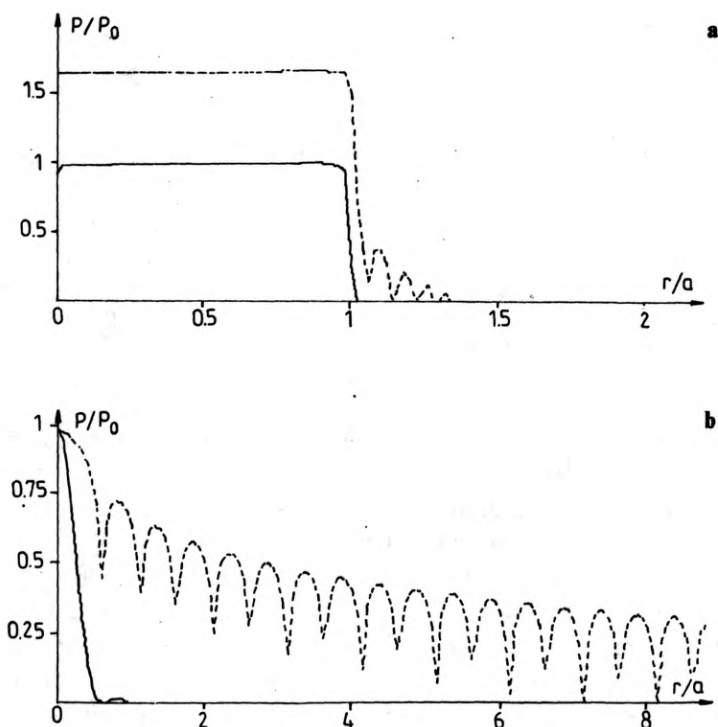


Fig. 13. Graphs of radiation power density. a — in the object plane, b — in the focal plane of the filter. Lower curve — linear scale, upper curve — logarithmic scale

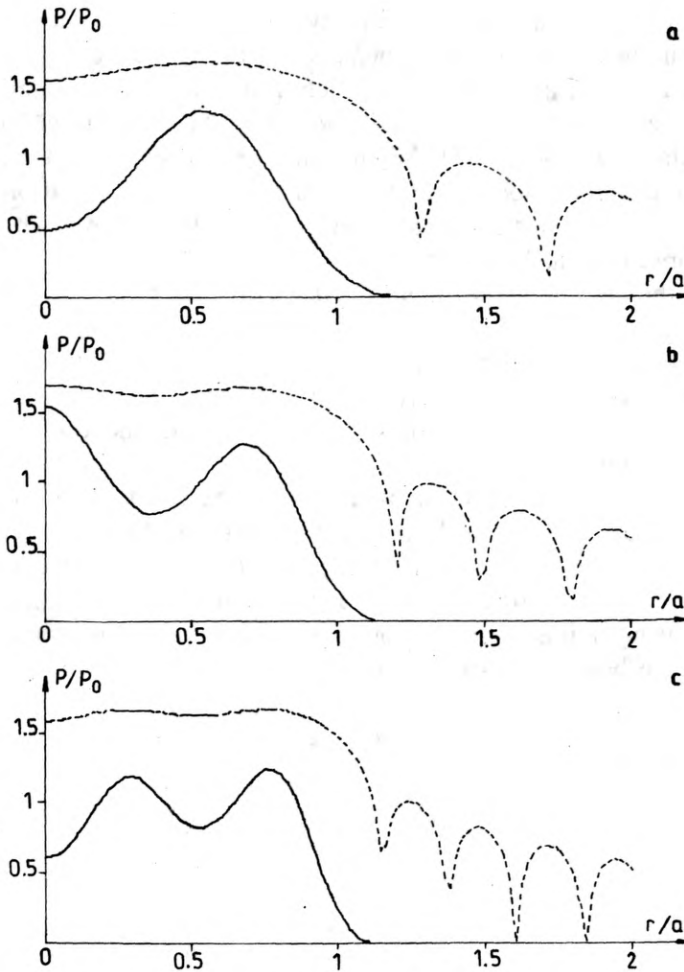


Fig. 14. Influence of the radius of the pinhole located at the focus on the power density distribution at the image plane. **a** – one side order passes through the pinhole, **b** – two side orders pass through the pinhole, **c** – three side orders pass through the pinhole

known Gibbs effect in numerical methods. Outside the central part of the beam in the image plane the low energy tail of the amplitude of order of 1% of average power density is visible in the central beam. This tail appears as a result of filtration. Due to low power this part of the beam will be amplified linearly in the laser rods and thus much stronger than the central part. Besides, the radiation may suffer from reflection from the surface of the side rods. The interference of this radiation and its strong amplification connected with oscillation structure of the power density at the rims of the beam may lead to perturbation of the uniform distribution in the amplified beam. With the increase of the pinhole radius the oscillation frequency increases outside the central part of the beam as well (see Fig. 15). Hence, it follows that for the design of the spatial filter these oscillations should be taken into account. They

should be eliminated, for instance, by inserting the suitable diaphragm in the beam trajectory through the amplifying head. The radius of the diaphragm should be equal to, e.g., the radius of the first minimum appearing outside the central part of the beam. The radius of the beam defined as the radius of the first minimum outside central part (in Fig. 15, for instance, it amounts to about 10.5 mm) is greater than it would follow from the geometrical optics. This phenomenon should also be taken into account when designing the spatial filters.

In the subsequent series of calculations the pinholes, were positioned in front of the focus plane (at about 22 mm in front of the focus) in the plane, for which the Fresnel number was equal to 2.

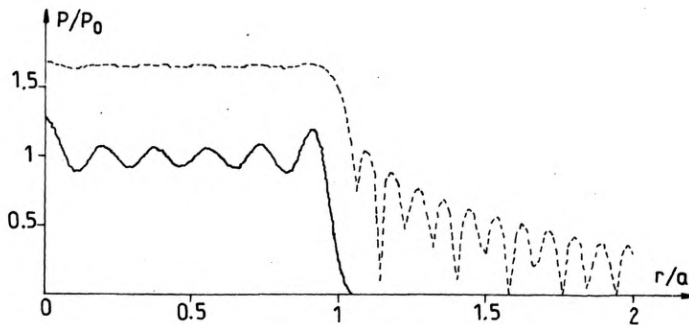


Fig. 15. Power density distribution of the radiation in the image plane of the filter. The pinhole of the radius 0.59 mm (equal to the radius of the 10th Airy ring) is located in the focal plane

In Figure 16 the distribution in the image plane of the filter has been plotted. The pinhole radii have been assumed to be the same as for the Fig. 14, i.e., 0.12, 0.17 and 0.22 mm. In this position ($F = 2$) and for such small radii of the pinhole, the differences decrease. In Figure 17 the distribution of the image plane of the filter occurring due to the filtration by the filter of radius of 0.53 mm (identical as in Fig. 15) has been plotted but for changed position of the pinhole ($F = 2$). When comparing Figs. 15 and 17 it can be seen that the differences are small now. The amplitudes and the oscillation frequency are also similar in the low energy part of the beam.

The shift of the pinhole to the plane defined by the Fresnel number $F = -2$ (i.e., toward the second lens of the filter) caused no changes in the distribution as compared to the position $F = 2$ except for the sign of the imaginary part of the electric field strength, which has been changed. The absolute values of the real and imaginary parts were exactly the same.

The above conclusions have been drawn after assuming high idealization of the laser beam. Among others, the restricted degree of coherence has not been accounted, which had significant influence on the distribution in the focus, and thus on the result of filtration.

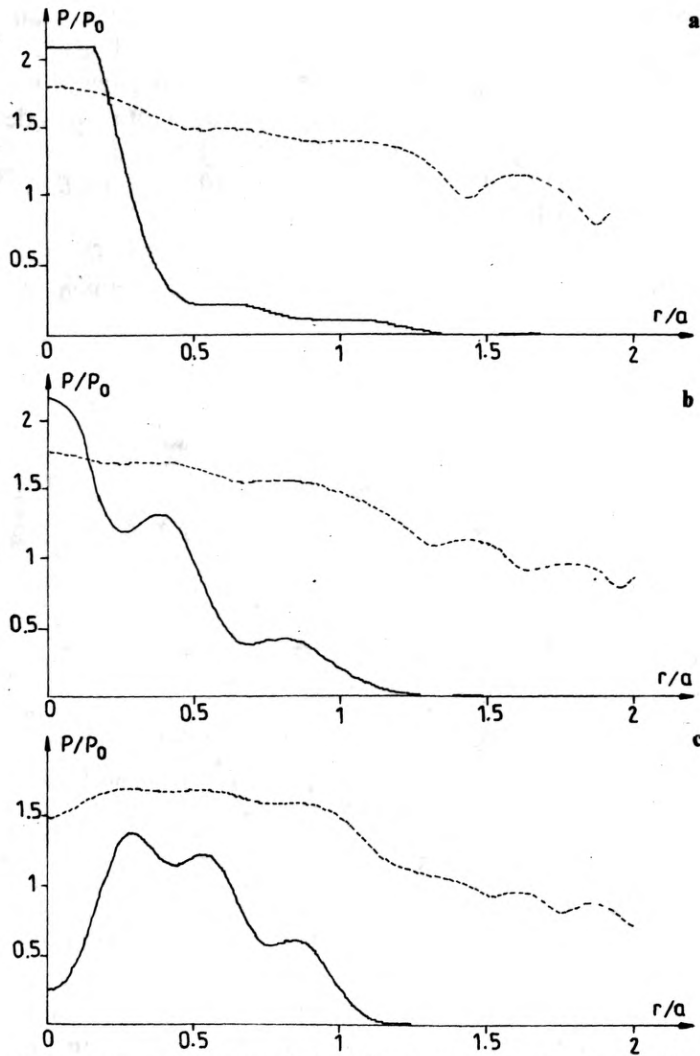


Fig. 16. Influence of the pinhole radius on the power density distribution at the filter image plane. The pinhole is located in the plane defined by the Fresnel number $F = -2$ (about 22 mm in front of the focal plane). Pinhole radius: a - 0.12 mm, b - 0.17 mm c - 0.22 mm

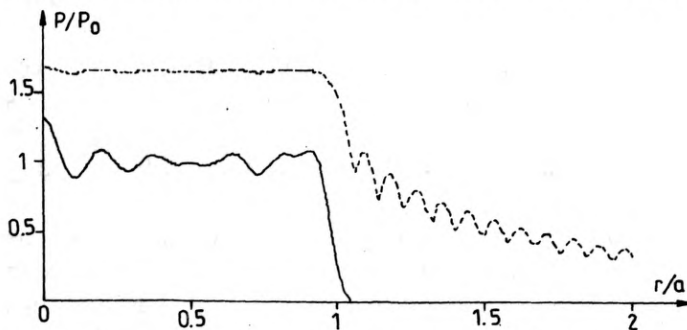


Fig. 17. Power density distribution of the radiation in the image plane of the filter. The pinhole is located in the plane defined by the Fresnel number $F = -2$. The pinhole radius 0.59 mm

5. Summary

In the examples given above, the effectiveness of the method of Laguerre–Gauss functions as applied to examinations of filtration and decoherencing has been illustrated. Thanks to this method considerable abridgement of the computing time of the radiation propagation in filters has been achieved. However, for the case of amplifiers, where it is necessary to determine the expansion coefficients in several planes, the computing time with this method becomes much longer as compared to that needed for the difference method. The final balance, however, speaks in favour of the method of eigenfunctions which offers much higher accuracy. In the examples considered, the minimal number of terms and r_m which assure the sufficient accuracy (but no higher than required) has not been examined. Thus, there exists a reserve which may allow us to model the work of a laser system with the needed accuracy.

References

- [1] DUBIK A., SARZYŃSKI A., *Opt. Appl.* 17 (1987), 211.
- [2] SIEGMAN A. E., *Opt. Lett.* 1 (1977), 13.
- [3] SIEGMAN A. E., SZIKLAS E. A., *Appl. Opt.* 13 (1974), 2775.
- [4] SIMMONS W. W., HUNT J. T., WARREN W. E., *J. Quant. Electr.* QE-17 (1981), 1727.
- [5] TALANOV V. I., *JETP Lett.* 11 (1970), 199.
- [6] DANILOV A. E., ORLOV V. V., SAVTSCHENKO S. M., SKLIZKOV G. V., FIEDOTOV S. I., CHITROV A. L., Preprint FIAN 136 (1985).

*Received October 22, 1987
in revised form February 29, 1988*

Применение метода функции Лагера–Гаусса для анализа линейного распространения излучения

В работе описан метод решения однородного и стационарного параболического уравнения (описывающего дифракцию излучения) основан на использовании собственных функций этого уравнения. Принято цилиндрическую симметрию пучка. Проверено влияние количества используемых собственных функций на точность аппроксимации начального условия. Проведено сравнение решений полученных методом собственных функций с решениями полученными разностным методом. Даны два примера использования метода: моделирование влияния когерентности на лазерный пучок и пространственная фильтрация.